

Influence of specimen dimensions on the tensile behavior of ultrafine-grained Cu

Enrique Lavernia


Scripta Materialia

Cite this paper

Downloaded from [Academia.edu](#) 

[Get the citation in MLA, APA, or Chicago styles](#)

Related papers

[Download a PDF Pack](#) of the best related papers 



[Influence of specimen dimensions and strain measurement methods on tensile stress-strain](#)

Deepti Rao

[Tensile deformation characteristics of bulk ultrafine-grained austenitic stainless steel produced by t...](#)

Dierk Raabe

[Enhanced tensile ductility of an ultra-fine-grained aluminum alloy](#)

Y. Estrin, I. Sabirov



Influence of specimen dimensions on the tensile behavior of ultrafine-grained Cu

Y.H. Zhao,^{a,*} Y.Z. Guo,^{b,c} Q. Wei,^b A.M. Dangelewicz,^d C. Xu,^e Y.T. Zhu,^f
T.G. Langdon,^{e,g} Y.Z. Zhou^a and E.J. Lavernia^a

^aDepartment of Chemical Engineering and Materials Science, University of California at Davis, Davis, CA 95616, USA

^bDepartment of Mechanical Engineering, University of North Carolina at Charlotte, Charlotte, NC 28223, USA

^cSchool of Aeronautics, Northwestern Polytechnical University, Xi'an, Shanxi, 710072, PR China

^dLos Alamos National Laboratory, Los Alamos, NM 87545, USA

^eDepartments of Aerospace and Mechanical Engineering and Materials Science, University of Southern California, Los Angeles, CA 90089-1453, USA

^fDepartment of Materials Science and Engineering, North Carolina State University, Raleigh, NC 27695-7919, USA

^gMaterials Research Group, School of Engineering Sciences, University of Southampton, Southampton SO17 1BJ, UK

Received 7 May 2008; revised 13 May 2008; accepted 14 May 2008

Available online 4 June 2008

Miniature dog-bone specimens with different sizes and geometries are frequently used to measure the tensile behaviors of nanostructured materials. Here we report a significant specimen dimensions influence on the tensile behavior of ultrafine-grained Cu: the elongation to failure, post-necking elongation and strain hardening rate all increase with increasing thickness or decreasing gauge length. The thickness effect is caused by the necking geometry and the effect of gauge length originates from the strain definition. © 2008 Acta Materialia Inc. Published by Elsevier Ltd. All rights reserved.

Keywords: Ultrafine-grained Cu; Specimen size and geometry; Tensile ductility; Finite element modeling (FEM)

Recently, the diminished tensile ductility of bulk nanostructured (NS) materials at ambient temperature has become a great concern as it limits the applications of such materials [1,2]. Efforts have been undertaken to show that the ductility (elongation to failure) of NS materials is closely linked to their microstructures and could be improved by microstructure engineering [1,2]. In addition to the intrinsic microstructural features, some external conditions, such as strain rate and temperature, may also affect the ductility [1,2].

A survey of the literature shows that a great variety of specimens with different sizes and geometries have been used by different authors, primarily depending on the availability of material. In many cases, the specimens deviate from the sizes and geometries dictated by ASTM standards [3]. For instance, the dog-bone thickness/width usually ranges from 100 μm [4] to several millimeters [5], and the gauge length from 1 mm [6] to several tens of millimeters [5]. This situation naturally invites

concern as to whether the tensile behaviors measured using such non-standard specimens are comparable. Accordingly, it is necessary to ask whether the geometries/dimensions of dog-bone specimens have any influence on the experimental results and, if so, how strong these influences are. To date, the only comparisons that can be made are directly between reported data, without considering the sample size effect [1,2,7].

A gradient-free size effect has recently become a topic of great interest as testing on nano- and micropillars has shown a strong size dependence of the strength of single crystals: the smaller the crystal, the stronger [8–11]. A large degree of plasticity has been observed by tensile testing Si nanowires [12] and even amorphous nanospecimens [13]. An increase in yield strength and a decrease in tensile ductility with decreasing specimen thickness were reported in free-standing Cu, Al, Au and Ni foils with thicknesses below 250 μm or even in the sub-micrometer range, and with grain sizes in the micrometer range [14–18]. Moreover, molecular dynamics (MD) simulation of Cu nanowires indicated that the yield stress decreased while ductility increased with increasing

* Corresponding author. E-mail: ytzhu@ncsu.edu

nanowire diameter due to the enhanced opportunities for dislocation motion at larger sizes [19]. Tests of the tension of single crystal Cu samples (with a diameter between 0.5 and 8 μm) found that strain hardening was negligible for long gauge specimens but pronounced for short gauge specimens due to sample geometry constrained glide of dislocations [20]. However, these specimen size effects may not extend to macroscopic NS tensile specimens with thicknesses above 250 μm and grain size below 1 μm , because various physical deformation mechanisms, operating on different length scales, govern the mechanical behavior of materials [21–23].

In this work, we investigated the influences of specimen size/geometry on the tensile behavior of pure ultra-fine-grained (UFG) copper (99.99%) prepared by equal-channel angular pressing via route Bc for eight passes. The grain/subgrain sizes in this UFG Cu are in the range of 100 nm–1 μm and the grains/subgrains are decorated by a high density of dislocations. Flat dog-bone specimens with different dimensions were sectioned by electro-discharge machining from the fully worked regions of the UFG Cu rods. Here we are primarily concerned with the following two scenarios. First, the specimen thickness (T) varies from $\sim 250 \mu\text{m}$ to $\sim 1.0 \text{ mm}$, while the gauge length (L) and width (W) are fixed at 1.0 and 2.0 mm, respectively. Second, L varies from 1.0 to 10.0 mm but T and W are fixed at 350 μm and 2.0 mm, respectively. Two sets of samples were prepared for every combination of T and L to ensure reproducibility. The flat surfaces of all the dog-bone specimens were polished using SiC papers to have a surface root mean square roughness of about 50 nm, as measured by atomic force microscopy. Tensile tests were performed on a Shimadzu Universal Tester with an initial quasi-static strain rate of $1.0 \times 10^{-3} \text{ s}^{-1}$. In parallel with the experimental analysis, finite element modeling (FEM) was used to simulate the specimen size effect on the tensile behaviors of dog-bone specimens. A bilinear constitutive model was adopted with yield stress of 400 MPa, a Young's modulus of 40 GPa, and a strain hardening modulus of 100 MPa. The values of L were 1.0, 2.0 and 4.0 mm at a constant T of 350 μm ; the values of T were 250, 350, 500 and 800 μm at a constant L of 1.0 mm. The W was 1.0 mm for all samples. During tension, one end of the specimen was fixed while the other end was subjected to a velocity load.

Figure 1 shows experimental (solid lines) and simulated (dashed lines) engineering stress–strain curves of the UFG Cu with an L of 1.0 mm and different values of T (as indicated in Fig. 1a), and with a fixed T of 350 μm and different values of L (as indicated in Fig. 1b). For all samples, strain softening (due to necking) occurred shortly after yielding, leading to a fast stress drop with strain, which is typical of UFG metals processed by severe plastic deformation because of the low dislocation storage capability. Both experiments and simulations suggest that when T increases from 250 μm to 1.0 mm (Fig. 1a) or L decreases from 10 to 1.0 mm (Fig. 1b), the necking portion (post-necking elongation) in the stress–strain curves of the UFG Cu is prolonged to a higher strain, resulting in a larger overall ductility. Moreover, reducing L and increasing T increases the apparent strain hardening rate without

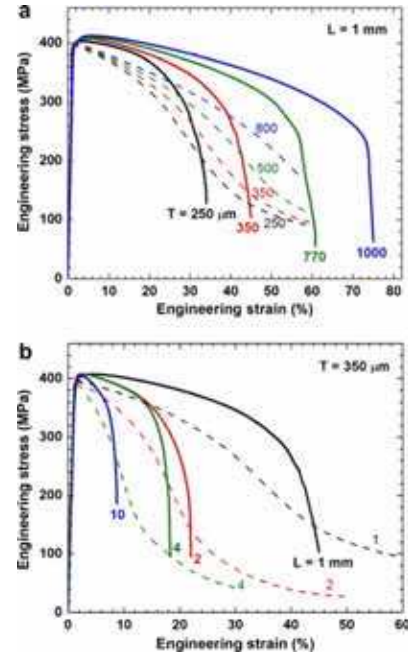


Figure 1. Experimental (solid lines) and simulated (dashed lines) results of the thickness T (a) and gauge length L (b) effects on engineering stress–strain curves of the UFG Cu with a width of 2 mm for experiment and 1 mm for simulation, respectively. The different thicknesses and gauge lengths are indicated in the figures.

changing the yield strength of UFG Cu, which is about 390 MPa. The thickness independence of the yield strength was also observed in nanocrystalline Ni by electrodeposits [24]. The discrepancy between simulations and experimental results is probably caused by the different gauge widths and the inhomogeneous structures in UFG Cu, which cause a vanishing strain hardening in the early stage of tension.

The uniform elongation ϵ_{ue} can be determined using the Considère criterion. The total ductility ϵ_{cf} , ϵ_{ue} and the post-necking elongation $\epsilon_{\text{pe}} (= \epsilon_{\text{cf}} - \epsilon_{\text{ue}})$ of the UFG Cu are shown in Figure 2 against T and L . The post-necking part accounts for a significant fraction of the total ductility. Both T and L tend to have significant effects on the post-necking elongation and the total ductility, but with no evident influence on the uniform elongation. The ϵ_{cf} (ϵ_{pe}) decreases from 75% (70%) to 34% (31%) with a reduction in T from 1.0 mm to 250 μm , and from 45% (41%) to 9% (7%) with an increase in L from 1.0 to 10 mm.

In order to understand the above specimen dimension/geometry effects on the tensile behavior of the UFG Cu, we performed scanning electron microscopy (SEM) and FEM analyses on failure processes. Figure 3 displays the effects of T and L on the failure mode and area reduction. With increasing T , the failure mode of the UFG Cu with an L of 1.0 mm changes gradually from shear to normal tensile failure, as shown in the insets in Figs. 2a and 3. When T of the specimen is increased from 250 μm to 1.0 mm, the angle between the failure plane and the loading axis increases from $\sim 55^\circ$ to $\sim 83^\circ$ and the area reduction increases from about 70% to 90%. These results suggest that thinner samples

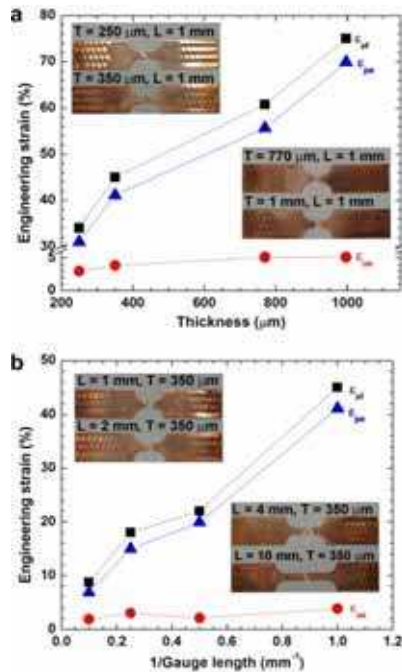


Figure 2. Thickness (a) and gauge length (b) effects on elongation to failure ϵ_{ef} , uniform elongation ϵ_{ue} and post-necking elongation ϵ_{pe} of the UFG Cu. The insets are the fractured tensile specimens with different thicknesses ($L = 1$ mm) and gauge lengths ($T = 350$ μm), as indicated in the figures.

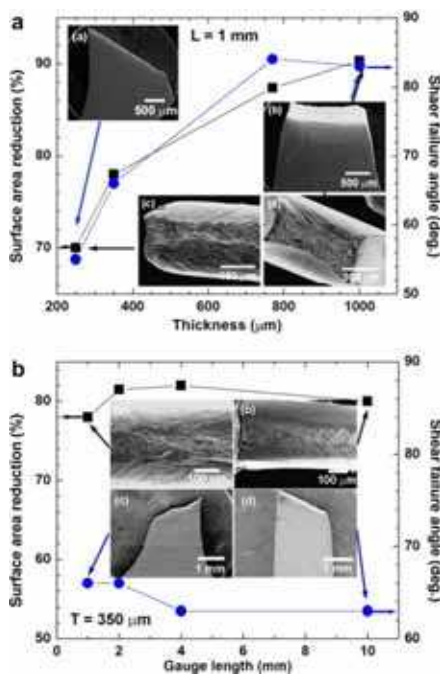


Figure 3. Thickness (a) and gauge length (b) effects on fracture surface area reduction and shear failure angle of the UFG Cu. The insets are SEM images of the fracture orientations and surfaces of the UFG Cu with $L = 1$ mm and $T = 250$ μm and 1 mm, respectively (a), and $T = 350$ μm and $L = 1$ and 10 mm, respectively (b).

are susceptible to shear failure, resulting in a smaller area reduction. However, the gauge length has no evi-

dent influence on the failure mode or area reduction, as shown in Figure 3b and the inset in Figure 2b. The UFG Cu specimens with a T of 350 μm and different L fractured with a shear failure angle of $\sim 63^\circ$ to 66° and an area reduction of about 80%.

The change in failure mode of the UFG Cu specimens vs. specimen thickness may be further explained by FEM simulations, as shown in Figure 4a–c. When specimens with $L = 1.0$ mm are pulled to the point of necking at an engineering strain of about 2%, two pairs of conjugated shear localizations appear at the gauge center of the sheet-like specimen (the T/W ratio is very small) (Fig. 4a). When T is 250 μm , the shear-band like structures combine to form a single coarsened shear band on the top plane of the gauge section (Fig. 4b). The shear angle to the tensile direction is about 50° , agreeing with the experimental value of $\sim 55^\circ$ for the UFG Cu with $T = 250$ μm . From the equivalent plastic strain (PEEQ) distribution at the side plane of the gauge part, one can see that shear deformation only occurs in the gauge top plane. However, when $T = 800$ μm , shear deformation is also observed on the gauge side plane (Fig. 4c). The interaction of the two series of shear bands (at both top and side planes) leads to a more complex stress state for the thicker specimens, giving rise to the experimentally observed normal fracture mode.

The change in tendency to necking with T originates from the specimen geometry, or more specifically from the T/W ratio. For thin, sheet-like specimens (T/W small), necking only occurs along the direction of T (insets in Fig. 3). When the T/W is close to unity (or T is comparable to W), necking occurs in both the W and T directions. An SEM analysis indicates that when $T = 1.0$ mm, necking reduces the thickness by 63% and the width by 49%. When $T = 250$ μm , necking reduces the thickness by 72% and the width only by about 15%. Large necking at $T = 1.0$ mm results in a large necking length in the tensile direction (inset b in Fig. 3a), rendering prolonged post-necking strain in the stress–strain curves. In addition to the specimen geometry limitation to the necking ability, surface defects (roughness and the deformation layer caused by grinding) will also reduce the necking ability by premature failure and such an influence will become more significant with decreasing T .

The gauge length effect on the measurement plastic strains can be explained by recourse to the definition of the engineering strain: $\epsilon = \Delta l/l_0$, where Δl is the apparent elongation, which is the summation of $\Delta l_1 + \Delta l_2 + \Delta l_3$ (Δl_1 is the elastic elongation, Δl_2 the uniform plastic elongation and Δl_3 plastic elongation by necking) and l_0 is the initial gauge length. For the UFG Cu, contributions from Δl_1 and Δl_2 are usually negligible. Post-loading SEM observations suggest that the gauge length has no evident effect on the failure mode and necking process, as further verified by Figure 4d–f. The necking area is about 1.0 mm in width (same as the width of the specimen) after maturation. These results imply that Δl_3 is independent of gauge length. Therefore, Δl is almost the same for different L under similar stress conditions and ϵ is inversely proportional to l_0 . This was further verified by Figure 2b. Both ϵ_{ef} and ϵ_{pe} of the UFG Cu have linear relationships with

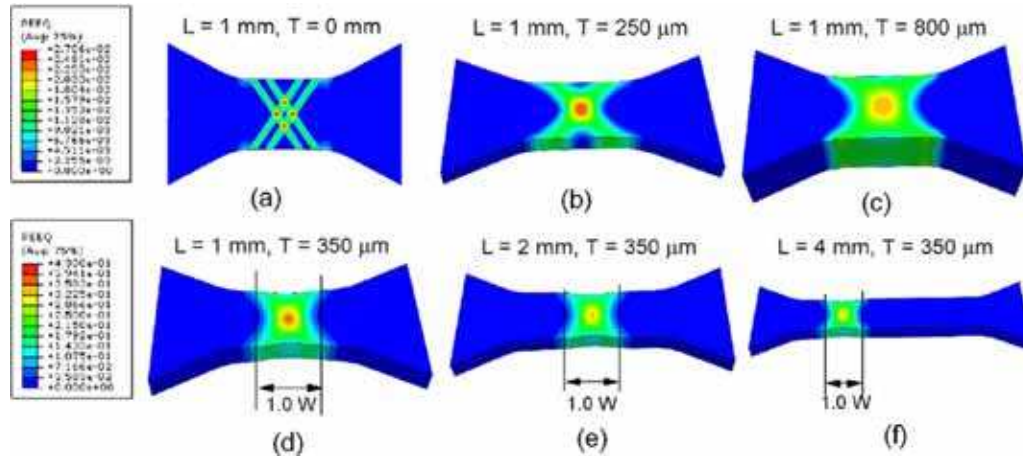


Figure 4. FEM results on thickness (a–c) and gauge length (d–f) effects on the equivalent plastic strain (PEEQ) distribution at the specimens. (a–c) PEEQ distributions of the specimens with $L = 1$ mm and $T = 0, 250$ and 800 μm at 2% engineering strain. (d–f) PEEQ distributions of the specimens with $T = 350$ μm and gauge lengths of 1, 2 and 4 mm, at 0.16 mm elongation (Δl).

l_0^{-1} . By extrapolating the ε_{pe} and ε_{ef} vs. l_0^{-1} curves to $l_0^{-1} = 0$, we find that $\varepsilon_{pe} \approx 0$ and $\varepsilon_{ef} \approx 3\%$ (ε_{ue}). This means that an infinite l_0 tends to nullify the post-necking strain and the failure strain is then the same as the uniform strain.

In summary, we have demonstrated that apparent tensile specimen dimension/geometry effects exist for the measured mechanical behavior of UFG Cu; specifically, we find that shorter and thicker specimens tend to be more ductile. The thickness effect is mainly caused by the necking geometry and/or fracture modes, and the gauge length effect originates from the strain definition. Our results and analyses suggest that the tensile specimen size effect should be considered when comparing mechanical properties, particularly tensile ductility, measured on non-standardized dog-bone specimens. Furthermore, we propose that, due to the ever-increasing popularity of miniaturized tensile specimens in research on UFG and NS materials, a standardized protocol should be adopted for use by the community at large.

Y.H.Z., Y.Z.Z. and E.J.L. would like to acknowledge support by the Office of Naval Research (Grant Number N00014-04-1-0370, N00014-08-1-0405), with Dr. Lawrence Kabacoff as program officer, and thank Prof. R.Z. Valiev for providing UFG Cu samples.

- [1] C.C. Koch, K.M. Youssef, R.O. Scattergood, K.L. Murty, *Adv. Eng. Mater.* 7 (2005) 787.
- [2] E. Ma, *JOM* 58 (4) (2006) 49.
- [3] <http://www.astm.org>.
- [4] Y.H. Zhao, J.F. Bingert, X.Z. Liao, B.Z. Cui, K. Han, A.V. Serhuceva, A.K. Mukherjee, R.Z. Valiev, T.G. Langdon, Y.T. Zhu, *Adv. Mater.* 18 (2006) 2494.

- [5] V.L. Tellkamp, A. Melmed, E.J. Lavernia, *Metall. Mater. Trans. A* 32 (2001) 2335.
- [6] K.M. Youssef, R.O. Scattergood, K.L. Murty, J.A. Horton, C.C. Koch, *Appl. Phys. Lett.* 87 (2005) 091904.
- [7] Y.T. Zhu, X.Z. Liao, *Nat. Mater.* 3 (2004) 351.
- [8] M.D. Uchic, D.M. Dimiduk, J.N. Florando, W.D. Nix, *Science* 305 (2004) 986.
- [9] C.A. Volkert, E.T. Lilleodden, *Philos. Magn.* 86 (2006) 5567.
- [10] J. Biener, A.M. Hodge, J.R. Hayes, C.A. Volkert, L.A. Zepeda-Ruiz, A.V. Hamza, F.F. Abraham, *Nano Lett.* 6 (2006) 2379.
- [11] A. Rinaldi, P. Peralta, C. Friesen, K. Sieradzki, *Acta Mater.* 56 (2008) 511.
- [12] X.D. Han, K. Zheng, Y.F. Zhang, X.N. Zhang, Z. Zhang, Z.L. Wang, *Adv. Mater.* 19 (2007) 2112.
- [13] H. Guo, P.F. Yan, Y.B. Wang, J. Tan, Z.F. Zhang, M.L. Sui, E. Ma, *Nat. Mater.* 6 (2007) 735.
- [14] M. Klein, A. Hadrboletz, B. Weiss, G. Khatibi, *Mater. Sci. Eng. A* 319 (2001) 924.
- [15] A. Hadrboletz, B. Weiss, G. Khatibi, *Int. J. Fract.* 109 (2001) 69.
- [16] H.D. Espinosa, B.C. Prorok, B. Peng, *J. Mech. Phys. Solids* 52 (2004) 667.
- [17] G. Simons, Ch. Weippert, J. Dual, J. Villain, *Mater. Sci. Eng. A* 416 (2006) 290.
- [18] Y. Yang, N. Yao, W.O. Soboyejo, C. Tarquinio, *Scripta Mater.* 58 (2008) 1062.
- [19] W. Liang, M. Zhou, *Proc. Inst. Mech. Eng. C* 218 (2004) 599.
- [20] D. Kiener, W. Grosinger, G. Dehm, R. Pippan, *Acta Mater.* 56 (2008) 580.
- [21] Z.P. Bazant, *PNAS* 101 (2006) 13400.
- [22] K. Sieradzki, A. Rinaldi, C. Friesen, P. Peralta, *Acta Mater.* 54 (2006) 4533.
- [23] G. Dehm, C. Motz, C. Scheu, H. Clemens, P.H. Mayrhofer, C. Mitterer, *Adv. Eng. Mater.* 8 (2006) 1033.
- [24] H. Wei, G.D. Hibbard, G. Palumbo, U. Erb, *Scripta Mater.* 57 (2007) 996.